Cross sections for production of the 15.10-MeV and other astrophysically significant gamma-ray lines through excitation and spallation of ^{12}C and ^{16}O with protons

F. L. Lang and C. W. Werntz
Code 682, Solar Physics Branch, Laboratory for Astronomy and Solar Physics, NASA/Goddard Space Flight Center, Greenbelt, Maryland 20771 and Department of Physics, The Catholic University of America, Washington, D.C. 20064

C. J. Crannell and J. I. Trombka
Code 682, Solar Physics Branch, Laboratory for Astronomy and Solar Physics, NASA/Goddard Space Flight Center, Greenbelt, Maryland 20771

C. C. Chang
Department of Physics and Astronomy, University of Maryland, College Park, Maryland 20742
(Received 18 August 1986)

The ratio of the flux of 15.10-MeV gamma rays to the flux of 4.438-MeV gamma rays resulting from excitation of the corresponding states in ^{12}C is a sensitive measure of the spectrum of the exciting particles produced in solar flares and other cosmic sources. These gamma rays are produced predominantly by interactions with ^{12}C and ^{16}O, both of which are relatively abundant in the solar photosphere. Gamma-ray production cross sections for proton interactions have been reported previously for all important channels except for the production of 15.10-MeV gamma rays from ^{16}O. The first reported measurement of the 15.10-MeV gamma-ray production cross section from $p+^{16}O$ is presented here. A cyclotron was employed to produce 40-, 65-, and 85-MeV protons which interacted with CH_2 and BeO targets. The resultant gamma-ray spectra were measured with a high-purity germanium semiconductor detector at 70, 90, 110, 125, and 140 deg relative to the direction of the incident beam for each proton energy. Other gamma-ray lines resulting from direct excitation and spallation reactions with ^{12}C and ^{16}O were observed as well, and their gamma-ray production cross sections, several of which have not been reported previously, are presented. The results are compared with previously reported measurements, as available.

I. INTRODUCTION

Nuclear gamma-ray line emission provides the most direct evidence available for the investigation of mechanisms by which protons and other ions are accelerated and interact in astrophysical sources, particularly solar flares. Gamma rays are unaffected by solar magnetic fields and carry unaltered information on characteristics of the accelerated-particle population as well as on the isotopic composition of the ambient medium in which the energetic particles interact. The current status of these investigations with respect to the Sun is presented in a review by Chupp.[1]

Because most nuclear levels above 8 MeV lead to little or no gamma-ray emission, studies of emission from solar flares have focused on the energy range below 8 MeV. There is, however, unique and valuable information to be learned from observations of high-energy line emission. For example, a pair of gamma-ray lines from states with widely separated production thresholds can provide a measure of the spectrum of particles accelerated in a flare. The most promising candidate states are the 2^+, $T=0$ level at 4.439 MeV and the 1^+, $T=1$ level at 15.11 MeV, both in ^{12}C.[2] However, both excited states can be produced by spallation reactions with ^{16}O as well as by inelastic (p,p′) scattering from ^{12}C. In the present work, measurements of the gamma-ray production cross section for the reaction $^{16}O(p,\gamma_{15,10})x^{12}C$ are reported for the first time. The ratio of the gamma-ray production cross sections for the two lines differs for the two nuclei, so that the flux ratio of the two lines in solar flares is dependent on the relative isotopic abundance as well as the proton spectrum.

Measurements of the differential gamma-ray production cross sections were obtained using the University of Maryland cyclotron. The gamma rays were measured with a high-purity germanium (HPGe) semiconductor detector. Spectra, covering the energy range from 50 keV to 20 MeV, were obtained with two targets for each energy and angle. A beryllium oxide target was employed for the oxygen cross section. A polyethylene target was employed to obtain measurements of the known carbon cross sections so that cross sections in oxygen could be determined as ratios to the corresponding cross sections in carbon, thus minimizing the effects of systematic uncertainties on the desired measurements.

Production cross sections for all lines of interest were determined from the measured spectra with detector efficiencies calculated with a Monte Carlo technique by Seltzer.[3] All cross sections were normalized by comparison of the $^{12}C(p,\gamma_{4.438})p'\,^{12}C$ cross section for 40-MeV protons measured in the present work with previously reported excitation cross sections. The results reported here include a self-consistent resolution of discrepancies in previously reported results. A major conclusion of this work, however, is that discrepancies in some of the cross sec-

tions remain large compared to the accuracy desired for the determination of spectral parameters and isotopic abundances in astrophysical settings.

The instrumentation and experimental techniques employed in the present work are discussed in the following section. Knowledge of the shape of the 4.438-MeV line from ^{16}O was required for the extraction of the corresponding gamma-ray production cross section, and a theoretical method for predicting the shape of this line is described in Sec. III. The analytic techniques used to determine the desired gamma-ray production cross sections from measured spectra are described in Sec. IV. In Sec. V the 15.10- and 4.438-MeV gamma-ray production cross sections are presented for both targets, as well as for the reaction $^{16}O(p,\gamma_{6.129})p'\,^{16}O$. In addition, the first resolved measurements of the gamma-ray production cross sections for the reactions $^{16}O(p,\gamma_{5.269})pp^{15}N$, $^{16}O(p,\gamma_{5.240})x^{15}O$, $^{16}O(p,\gamma_{5.105})x^{14}N$, $^{16}O(p,\gamma_{2.793})x^{14}N^*(2.313)$, $^{16}O(p,\gamma_{2.740})p'\,^{16}O^*(6.130)$, $^{16}O(p,\gamma_{2.313})x^{14}N$, and $^{12}C(p,\gamma_{2.000})x^{11}C$ are reported. The gamma-ray lines from the reactions $^{12}C(p,\gamma_{2.154})x^{10}B$ and $^{12}C(p,\gamma_{2.124})pp^{11}B$ could not be resolved, but the sum of the cross sections is presented. Section VI is a summary of the results obtained and the remaining related requirements for astrophysical applications.

II. EXPERIMENTAL METHOD

The data presented in this paper were obtained using the University of Maryland Sectored Isochronous Cyclotron Facility at a low background station especially designed for gamma-ray measurements. Beams of 40-, 65-, and 85-MeV protons generated with the cyclotron were directed at three solid targets. Pulse-height spectra were obtained with a high-purity germanium semiconductor at 70, 90, 110, 125, and 140 deg relative to the direction of the incident beam for each proton energy.

The proton beam was pulsed, with a width of 1 ns at a repetition rate determined by the ratio frequency (rf) of the cyclotron (one pulse every 60 to 90 ns depending on the proton energy). The transmitted beam current was measured with a Faraday cup attached to the beam pipe downstream of the target chamber. The beam line, target, and gamma-ray detector arrangement are shown schematically in Fig. 1.

Thin foils of polyethylene (CH_2), beryllium oxide (BeO), and beryllium (Be) were employed as targets. Each of these foils was held in an aluminum target frame which comprised a remotely changeable, three-element target ladder oriented at 45 deg to the incident beam. The three targets presented thicknesses of 18 ± 2 mg/cm^2 (^{12}C), 50 ± 5 mg/cm^2 (^{16}O), and 18 ± 2 mg/cm^2 (Be) to the proton beam, respectively. Because no intense gamma-ray lines are produced by proton interactions with beryllium, the pulse-height spectra obtained with the beryllium target were used only to verify that the proton beam was not hitting the aluminum target frame.

The gamma rays were detected with a high-resolution semiconductor device consisting of high-purity germanium (HPGe) located 1.9 m from the target. The HPGe detector is a cylinder 58 mm in diameter by 46 mm in height. Due to neutron damage sustained prior to these measurements, this detector had a relatively poor spectral resolution of about 7 keV full width at half maximum (FWHM) at 1.332 MeV. As located, it subtended a solid angle of 0.72 ± 0.02 msr. Corrections to the measured cross sections due to the aluminum window covering the detector and due to the germanium dead layer totaled less than 2%.

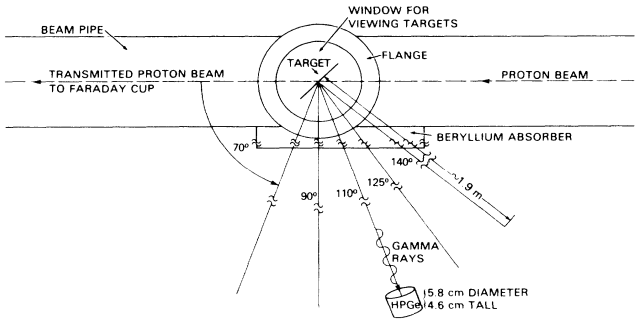

FIG. 1. This is a schematic diagram illustrating the experimental setup as seen from above.

A significant fraction of background events resulted from neutrons, protons, and other particles incident on the detector. A time-of-flight technique which measured the arrival time of each detector event with respect to the next rf signal (see Ref. 4 for a more detailed discussion) was used to eliminate most of these events. The time resolution of the instrumental system (the convolution of the beam pulse width with the intrinsic time resolution of the detector, along with all other factors) was measured to be 5 ns FWHM. A 10 ns time-of-flight gate resulted in better than a factor of 5 reduction of background from this source. The importance of this is seen in Fig. 2, which shows both the ungated pulse-height spectrum and the gated spectrum obtained by applying a time-of-flight window to the raw, ungated pulse-height spectrum. Background due to protons which scattered from the target and charged spallation products produced in the target not eliminated by the time-of-flight window was further reduced by placing beryllium shielding 14.2 ± 0.3 g/cm^2 thick between the target and the detector. The absorption of gamma rays by the beryllium shielding required an upward correction to the measured cross sections by a factor of 1.2—2.4.

The detector gain was very stable over all runs with a standard deviation of 0.2%. This was determined by comparison of the centroid of the photopeak at 6.129 MeV resulting from the decay of the 6.130-MeV level of ^{16}O and the centroid of the second-escape peak at 4.218 MeV resulting from the decay of the 5.241-MeV level of ^{15}O for all BeO target runs. The relatively long lifetime ($\tau > 1$ ps) of these two states allowed the excited nuclei to come to rest in the solid targets and the corresponding gamma-ray lines are intrinsically narrow. Because there are relatively few narrow lines observed in our spectra, these two proved to be very useful for monitoring the gain of the detector.

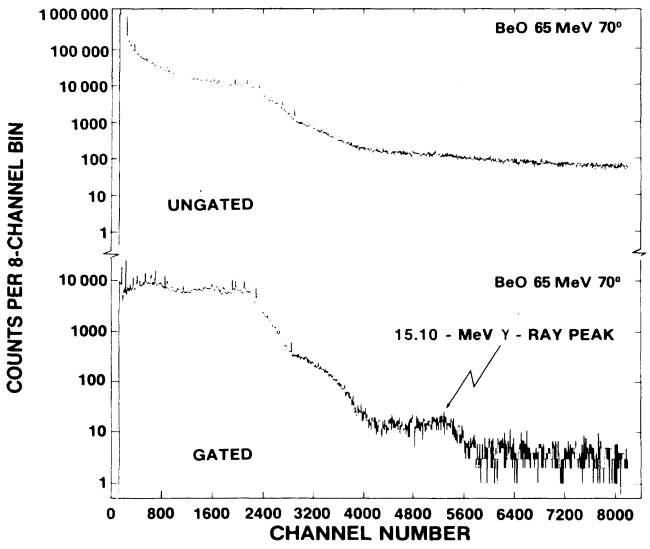

FIG. 2. A typical total pulse-height spectrum for 65-MeV protons incident on the BeO target both before and after gating by the time-to-amplitude converter (TAC) window. This spectrum was measured at 70 deg to the proton beam for approximately 1 h. Each histogram bin gives the total counts in eight raw pulse-height channels. The ungated spectrum is dominated by the large background of neutrons and delayed gamma rays. The gated spectrum clearly shows a significant increase in the signal to noise ratio. The enhancement of the 15.10-MeV gamma-ray line made possible the present measurement of the corresponding cross section.

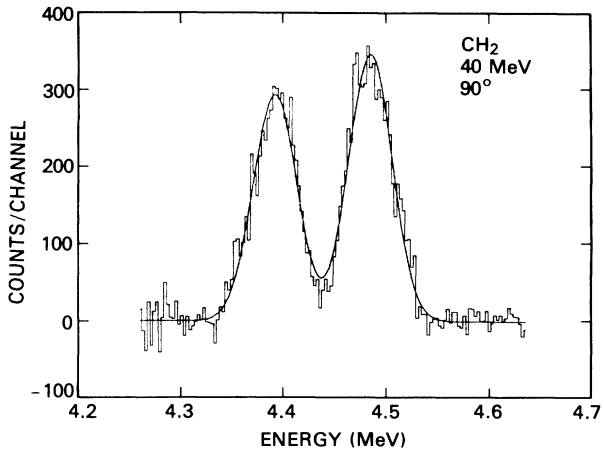

FIG. 3. Residuals (background has been subtracted) for a portion of the pulse-height spectrum obtained with 40-MeV protons incident on the CH_2 target measured at 90 deg to the proton beam. Each histogram bin gives the total counts in one raw pulse-height channel. Included is the split gamma-ray line at 4.438 MeV from the reaction $^{12}C(p,\gamma_{4.438})p'\,^{12}C$. Also shown as a solid line is the fit to the background and line complex using the template computed as discussed in Sec. IV A. The line profile is asymmetric because gamma rays measured at 90 deg to the proton beam in the lab frame correspond to gamma rays emitted at a slightly larger angle in the c.m. frame.

III. THEORETICAL LINE SHAPE FOR $^{16}O(p,\gamma_{4.438})p'\,\alpha^{12}C$

The width of a gamma-ray line produced in a (p,γ) reaction depends critically on whether the lifetime of the gamma-ray emitting state is less than or greater than the slowing down time of the recoiling ion in the target material. In a solid target, if the lifetime is of the order of picoseconds or longer, there will be no Doppler broadening; transitions of states with femtosecond or shorter lifetimes give rise to broad lines, the shapes of which are characteristic of the kinetics of the originating nuclear reaction. In order to extract the strength of a given transition from an experimental pulse-height spectrum in which the background can change over the width of such a line, it is advantageous to have a model for calculating the shape of the line.

These considerations are particularly relevant to the $^{12}C(p,\gamma_{4.438})p'\,^{12}C$ and $^{16}O(p,\gamma_{4.438})x^{12}C$ reactions. For example, in the former reaction the gamma-ray line observed at right angles to the initial proton beam direction in the laboratory frame is split into two nearly symmetric peaks (see Fig. 3). This so-called "coherent Doppler effect" was observed and the angular-dependent shape was related to magnetic sublevel populations by Kolata, Auble, and Galonsky.[5] Unfortunately, their parametrization of the line shapes is inadequate because they made the assumption that the diagonal elements of the $^{12}C^*$ magnetic substate density matrix completely determine the proton to gamma-ray angular correlation. The practical result is that the parameters needed to fit the shape at $\theta_\gamma = 90°$, three in number and relatively easy to extract from the data itself, are insufficient to predict shapes at forward or backward angles, for which additional parameters are required. Fortunately, an empirical knowledge of the intrinsic shape of this line is unnecessary to determine the differential gamma-ray production cross section. The same is not true of the latter reaction, for which the line shape must be computed analytically because, due to the presence of numerous nearby and overlapping lines observed with the HPGe detector, standard techniques were inadequate to consistently model the measured line profile.

Epstein *et al.*[6] studied the reaction $^{16}O(p,p'\alpha)^{12}C^*(4.439)$ with 46.8-MeV protons through energy measurements at fixed laboratory angles of protons and alpha particles in coincidence. They established that single-step direct action processes played virtually no role; the $^{12}C^*(4.439)$ are produced through the excitation of individual ^{16}O excited states which subsequently decay through the $^{12}C^*(4.439) + \alpha$ channel. Between ^{16}O excitation energies of 15 and 26 MeV, eleven individual peaks in Figs. 9 and 10 of Epstein *et al.*[6] have been identified in the present work. These peaks can be correlated with peaks in the inclusive $^{16}O(p,p')$ spectrum of Buenerd *et al.*[7] taken at 40 deg to their 45-MeV proton beam. In

addition, the data of the latter group show strong proton excitation of states at 12.53 (2^-), 13.26 (3^-), and 13.97 MeV (2^-), which have known[8,9] ratios of α_1 widths to total widths of 1.0, 0.25, and 0.50, respectively.

In order to calculate the Doppler-broadened shape of the line, the problem is initially treated in the overall $^{16}O + p$ c.m. frame. In the two-step process, the recoil velocity of $^{12}C^*(4.439)$ is the sum of $\beta_c(E_N)$, the velocity of the $^{16}O^*(E_N)$ in the overall c.m. frame, and $\beta(E_N)$, the velocity of the emitted $^{12}C^*(4.439)$ nucleus in the c.m. frame of the recoiling $^{16}O^*(E_N)$. In the overall c.m. frame, for $\beta_c \ll 1$ and $\beta \ll 1$, the distribution function for 4.438-MeV gamma rays being emitted in a direction θ_γ with a Doppler shift E_c following excitation of the ^{16}O target to an energy E_N is given by

$$N_c(\theta_\gamma,E_c,E_N)=\int\int d\hat{\beta}_c d\beta\, n(\hat{\mathbf{k}}_\gamma,\hat{\beta}_c,\beta) \times\delta(E_c-E_0[\beta_c(E_N)+\beta(E_N)]\cdot\hat{\mathbf{k}}_\gamma) . \quad (1)$$

The function $n(\hat{\mathbf{k}}_\gamma,\hat{\beta}_c,\beta)$ is proportional to the number of gamma rays emitted in the direction $\hat{\mathbf{k}}_\gamma$ when the $^{12}C^*(4.439)$ recoils with velocity $\beta_c(E_N)+\beta(E_N)$.

A close examination of the present data for the 4.438-MeV line reveals, at some angles, only a suggestion of the double-peak structure characteristic of the line that is observed when ^{12}C itself is the target. Therefore, it is likely that the sum over many levels of different J^π is equivalent to isotropic α decay of $^{16}O^*(E_N)$ followed by isotropic emission of a gamma ray by the excited carbon nucleus. Then,

$$n(\hat{\mathbf{k}}_\gamma,\hat{\beta}_c,\beta)\rightarrow\frac{\Gamma_{\alpha_1}(E_N)}{\Gamma_{\rm tot}(E_N)}\sigma(\theta_c,E_N)\frac{1}{4\pi}\frac{\delta(\beta-\beta_m(E_N))}{\beta_m^2(E_N)}\frac{1}{4\pi} , \quad (2)$$

where $\Gamma_{\alpha_1}(E_N)$ is the partial width for decay of the level through the $^{12}C^* + \alpha_1$ channel, $\Gamma_{\rm tot}(E_N)$ is the total width of the level, $\sigma(\theta_c,E_N)$ is the differential cross section for producing the level, and $\beta_m(E_N)$ is the velocity of the $^{12}C^*(4.439)$ in the $^{16}O^*(E_N)$ c.m. frame. The E_N may be considered to be discrete energies since the widths of the states are small compared to their excitation energies.

The gamma-ray distribution function given by Eq. (1) refers to the contribution of a single ^{16}O excited state of energy E_N in the c.m. frame of $^{16}O + p$. Under the condition that $\beta_{\rm c.m.} \ll 1$, the emission angle in the lab frame, θ'_γ, is little different from the emission angle in the c.m. frame, θ_γ. Summing over all contributing levels, the distribution function for gamma rays as a function of the laboratory Doppler shift E'_c becomes

$$N(\theta'_\gamma,E'_c)=\sum_N N_c(\theta'_\gamma,E'_c-\beta_{\rm c.m.}\cdot\mathbf{k}_\gamma,E_N) . \quad (3)$$

Here, $\beta_{\rm c.m.}$ is the laboratory velocity of the $^{16}O + p$ c.m. frame.

In order to use Eq. (3), the angular dependence of the differential proton scattering cross section at each energy must be known. Differential cross sections available in the literature at $E_p = 45$ MeV (Ref. 7) are limited to an average over the giant dipole region of ^{16}O. For the present work, their angular dependence at 45 MeV has been adopted for 40-MeV protons and has been assumed to be the same for all levels.

The proton differential cross section in Eq. (2) refers to the cross section for exciting a given isolated resonant state. Experimentally, these states appear as peaks up to a few hundred keV wide superposed on a background due primarily to (p,2p) and (p,pn) reactions. In their published spectrum, Buenerd *et al.*[7] used a straight line background which has the unphysical feature of being nonzero well below the threshold for $^{15}N + p$ and $^{15}O + n$. The analytic form which was substituted in this work is

$$\sigma_{\rm bg}=1.36\{\exp[-(31-E_N)^2/\mathscr{E}^2] +0.25\exp[-(26-E_N)^2/\mathscr{E}^2]\} , \quad (4)$$

where σ is in units of mb/(sr MeV) and $\mathscr{E}=7.2$ MeV. The two energy parameters in the background model were chosen to give a reasonable fit to the cross section above $E_N = 27$ MeV. This expression puts more strength for the ^{16}O level excitation in the 12–20 MeV interval than reported in Ref. 7, but still allows the background to account for all strength above 28 MeV.

Because the peaks above $E_N = 16$ MeV are overlapping in the (p,p') spectrum, it was necessary to divide the spectrum into 2-MeV wide bins centered at 17, 19, 21, 23, 25, and 27 MeV. While the ratio $\Gamma_{\alpha_1}/\Gamma_{\rm tot}$ averages 0.42 below 16 MeV for the well known states, it should become smaller above the opening of the $^{15}O + n$ channel at 15.67 MeV. Therefore, the central values of $\sigma(40°,E_N)\Gamma_{\alpha_1}(E_N)/\Gamma_{\rm tot}(E_N)$ reported in Table I were evaluated by assuming that $\Gamma_{\alpha_1}/\Gamma_{\rm tot}=\frac{1}{3}$. The procedure outlined above has been employed to compute the

TABLE I. Contributions of each energy state or region of the $^{16}O(p,p')^{16}O^*$ spectrum to the $^{16}O(p,\gamma_{4.438})x^{12}C$ reaction. Values of $\Gamma_{\alpha_1}(E_N)/\Gamma_{\rm tot}(E_N)$ are derived from Refs. 8–11, and the cross sections at 40 deg were taken from Ref. 7. Where pairs of states were unresolved, the shape of the experimental peak was fitted with the sum of two Breit-Wigner resonant shapes using the known total and partial width.

E_N (MeV)	$\Gamma_{\alpha_1}/\Gamma_{\rm tot}$	$(\Gamma_{\alpha_1}/\Gamma_{\rm tot})\sigma(40°,E_N)$ (mb/sr)
12.53	1.00	0.26
13.02	0.12	0.14
13.26		
13.97	0.42	0.25
15.27	0.43	0.88
15.50		
16–18	0.33	0.60
18–20	0.33	0.90
20–22	0.33	0.61
22–24	0.33	0.54
24–26	0.33	0.36
26–28	0.33	0.11

gamma-ray line profiles at five angles for 40-MeV protons incident on BeO for use in the next section for the determination of the gamma-ray line area for this reaction.

IV. CALCULATIONAL TECHNIQUES

A. Determination of gamma-ray line areas from measured spectra

A monochromatic beam of low-energy (less than about 8 MeV) gamma rays incident on a germanium detector will produce one or more features in the measured pulse-height spectrum. The photopeak corresponds to complete energy conversion of the gamma ray. For gamma rays with sufficient energy to pair produce, single- and double-escape peaks, located 0.51 and 1.02 MeV below the photopeak, also appear (see Fig. 4). Compton scattering also is an important energy-loss mechanism and is most noticeable as a shoulder located typically 200—250 keV below the photopeak of strong lines. A monochromatic beam of high-energy (greater than about 10 MeV) gamma rays incident on a germanium detector does not produce the same prominent features as do low-energy gamma rays. As is seen in Figs. 2 and 5, the 15.10-MeV gamma rays produced in the reactions $^{16}O(p,\gamma_{15.10})x^{12}C$ and $^{12}C(p,\gamma_{15.10})p'^{12}C$ result in a single, broad feature (greater than 1 MeV FWHM) in the pulse-height spectrum.

Three techniques have been employed to determine the area of features in the pulse-height spectra. The first technique, applied to all 15.10-MeV features, required the determination of two templates from the data. A single spectrum was first obtained by summing the five pulse-height spectra for 40-MeV protons incident on the CH_2 target into 20-channel bins. A linear background template was then constructed from the spectral region above 15.50 MeV in the same five-spectra sum. This was extrapolated to lower energies and subtracted from the five-spectra sum to yield the line template. The areas of individual peaks were determined by performing a least-squares fit[12] to the sum of the two templates, each multiplied by a variable amplitude. Simultaneously, the data were allowed to shift relative to the templates to allow for possible gain changes and for the intrinsic angular-dependent Doppler shifts. Two typical fits are shown in Fig. 5.

A second technique was employed to determine the areas of the photopeak features from the reaction $^{16}O(p,\gamma_{4.438})x^{12}C$. These photopeaks exhibit significant Doppler broadening, and the first-escape peak from the 5.105-MeV line is superposed on their high-energy tails (see Fig. 6). Escape peaks from the resolved 5.240- and 5.269-MeV narrow lines and the unresolved 5.182- and 5.300-MeV Doppler-broadened lines, all from ^{15}O and ^{15}N, bracket and partially overlap the 4.438-MeV photopeak. Standard analytic Gaussian techniques (see below) were initially applied to these photopeaks. The areas thus derived clearly exhibited systematic effects because the background and peak regions for this line were selected

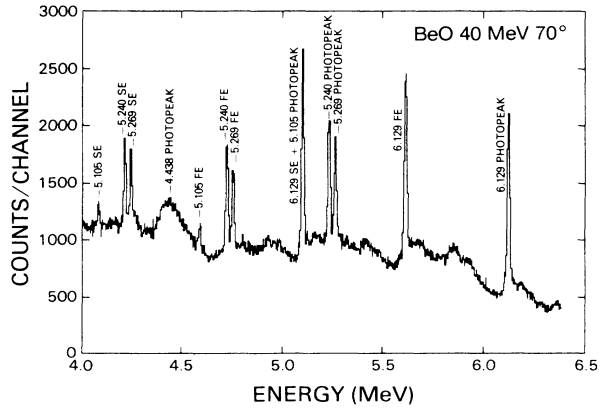

FIG. 4. A portion of a pulse-height spectrum for 40-MeV protons incident on the BeO target measured at 70 deg to the proton beam. Each histogram bin gives the total counts in one raw pulse-height channel. This portion includes the narrow gamma-ray lines at 6.129, 5.269, and 5.240 MeV along with their first-escape (FE) and second-escape (SE) peaks. Also evident are the narrow 5.105-MeV first- and second-escape peaks (the photopeak is coincident with the second-escape peak of the 6.129-MeV line) and the broad 4.438-MeV photopeak from ^{12}C.

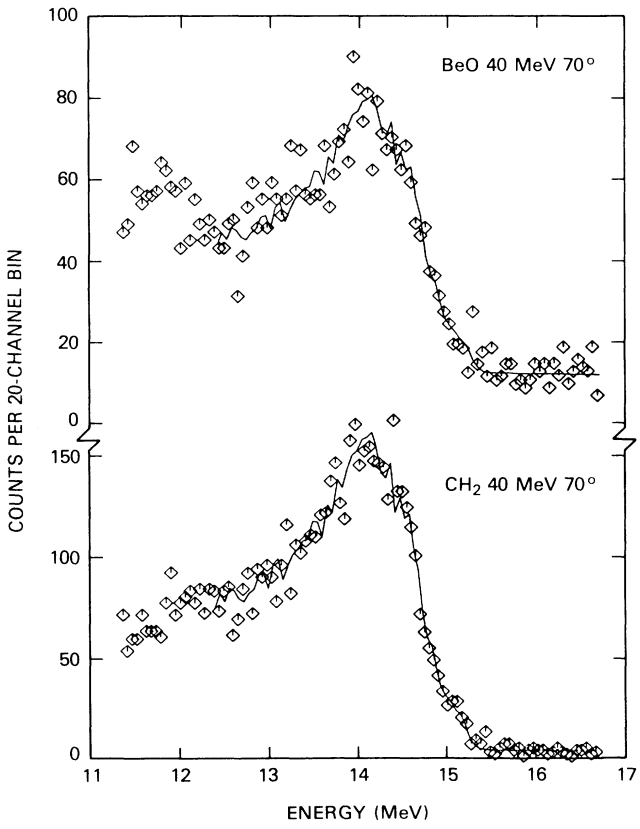

FIG. 5. Two typical 20-channel summed pulse-height spectra in the region of the 15.10-MeV gamma-ray line. Each diamond gives the total counts in 20 raw pulse-height channels. Also shown as a solid line is the fit to the background and line complex. The templates were derived from the data as discussed in the text.

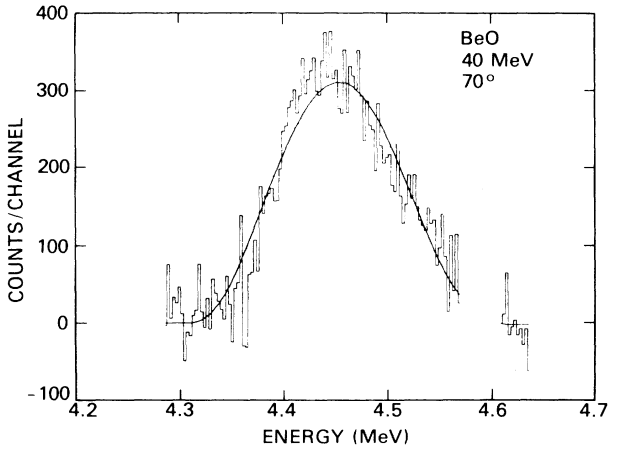

FIG. 6. Residuals (background has been subtracted) for a portion of the pulse-height spectrum obtained with 40-MeV protons incident on the BeO target measured at 70 deg to the proton beam. Each histogram bin gives the total counts in one raw pulse-height channel. Included is the broad gamma-ray line at 4.438 MeV from the reaction $^{16}O(p,\gamma_{4.438})x^{12}C$. Also shown as a solid line is the fit to the background and line complex using the template computed as discussed in Sec. III.

inconsistently due to the presence of the fixed-position narrow lines. For these reasons, a model for the 4.438-MeV line shape was derived as described in Sec. III. This model was employed to compute the expected gamma-ray line profiles at five angles only for 40-MeV incident protons. Broadening of the template due to the finite resolution of the detector is negligible. Each template was normalized to unit area and was fitted to the corresponding photopeak, simultaneously with a quadratic background. A sample fit is also shown in Fig. 6. The "gap" in the spectrum corresponds to the location of the first-escape peak of the 5.105-MeV gamma-ray line from ^{14}N and was excluded during the fit.

The remaining line areas were determined using one of two fitting procedures with Gaussian line shapes. The computer program HYPERMET (Ref. 13) provided one such procedure, and was employed in the initial determination of the photopeak areas of all of the remaining lines of interest. HYPERMET constructs a peak-shape function consisting of a Gaussian template and several small correction terms. A search is performed for significant peaks in the pulse-height spectrum. The peak-shape function, along with an underlying quadratic background, is fit to each peak. Chi-squared is computed for the fit, and further peaks are included if necessary.

The resulting photopeak areas were employed in the determination of the corresponding gamma-ray production cross sections, *except* for the 5.105-MeV line from the reaction $^{16}O(p,\gamma_{5.105})x^{14}N$ and the 4.438-MeV line from both targets. The 4.438-MeV line from the oxygen target has been discussed above. Because the photopeak from the 5.105-MeV line is not resolved from the second-escape peak from the 6.129-MeV line, the first-escape peak areas, also determined with HYPERMET, were selected for use in the determination of the corresponding cross sections.

HYPERMET was designed to determine areas for lines that are narrow relative to changes in the background. The intrinsic line profile from the reaction $^{12}C(p,\gamma_{4.438})p'^{12}C$ is quite broad and measured spectra show a strong rise in the background toward lower energies. The line profile could not be computed analytically, as was done for the reaction $^{16}O(p,\gamma_{4.438})x^{12}C$, because knowledge of the parameters for the correlation function was lacking.

A second estimate of the photopeak areas was obtained by the following procedure. Reduced pulse-height spectra were constructed by subtracting the best-fitted quadratic backgrounds derived by HYPERMET (Ref. 13) from the raw pulse-height spectra. The 4.438-MeV photopeaks in the reduced spectra were fitted to line shapes consisting of up to three Gaussians using a least-squares technique.[12] One- or two-Gaussian line shapes generally sufficed to simulate the reduced line profile. The values of chi-squared from the HYPERMET and multiple-Gaussian procedures were compared, and the area determined with the better-fitting procedure (about half from each) was selected as the best estimate of the photopeak area. Figure 3 shows a typical fit resulting from the multiple-Gaussian procedure.

Uncertainties in the measured areas due to unresolved Compton edges could affect only the broad 4.438-MeV lines. Because no strong lines had photopeaks in a position to result in Compton edges below the 4.438-MeV line, this effect could have no more than a 1% effect on the measured cross sections. No lines produced by neutron interactions in the detector lie above the lowest gamma-ray energy considered here (2.000 MeV).

B. Determination of gamma-ray production cross sections from gamma-ray line areas

The desired total gamma-ray production cross sections cannot be determined by straightforward integration of the measured differential cross sections. It can, however, be determined from the physics of the nuclear decay, in which the angular distribution of gamma rays is expected to be of the form

$$\sigma(\theta)=\sum_{l=0;\ l\ \text{even}}^{L} a_l P_l(\cos\theta)\ . \tag{5}$$

In Eq. (5), $P_l(\cos\theta)$ is the Legendre polynomial of order l, and the a_l's are parameters to be determined. The sum is performed over even values of l from zero to L, where L is the lesser of (i) twice the multipolarity of the gamma ray, and (ii) twice the spin of the decaying nuclear state. The total cross section is simply

$$\sigma_{\text{tot}}=4\pi a_0\ . \tag{6}$$

Because a number of the factors in $\sigma(\theta)$, such as the target thickness, the detector efficiency, and the solid angle, have significant uncertainties, the differential cross section was divided into an angular-dependent term and a "constant" term. By performing the angular fits to the

angular-dependent term only, uncertainties due to systematics and overall normalization have been separated from the statistical uncertainties, rendering the resulting angular distributions more meaningful. Figure 7 shows typical angular distributions of the angular-dependent term, in arbitrary units, plotted as a function of observation angle for selected lines. Also shown are the Legendre-polynomial fits, the coefficients of which are presented in Table II.

There are two small corrections to the angular-dependent term that have been neglected when fitting to the Legendre-polynomial series. The first, the variation of the Legendre polynomials over the gamma-ray detector area, would cause less than a 1% difference in the total

TABLE II. Legendre-polynomial coefficients for the measured angular distributions of the angular-dependent portion of $\sigma(\theta)$. The coefficients a_l in Eqs. (5) and (6) are proportional to the entries in this table. The constant of proportionality is a function of both the gamma-ray energy and the target material, but is not a function of the incident proton energy.

			Coefficient of P_l in expansion (arbitrary units)							
E_γ	Target	E_p	b_0	Error	b_2	Error	b_4	Error	b_6	Error
15.10	BeO	40	5.93	0.11	0.22	0.32				
		65	2.93	0.07	0.29	0.20				
		85	2.56	0.12	0.57	0.32				
	CH_2	40	13.47	0.15	1.77	0.43				
		65	7.92	0.12	1.70	0.33				
		85	5.76	0.13	1.87	0.38				
4.438	BeO	40	5.37	1.53	3.40	5.51	−4.95	5.55		
	CH_2	40	47.95	1.41	18.91	4.86	−0.65	4.49		
		65	18.34	1.00	2.55	3.29	−6.73	3.09		
		85	12.37	0.76	7.18	2.61	−4.11	2.88		
6.129	BeO	40	39.56	1.71	30.80	7.21	30.63	8.17	−5.04	4.55
		65	15.34	0.93	−0.53	3.89	−0.22	4.32	−10.50	2.53
		85	13.86	0.95	14.52	3.88	14.59	4.25	1.91	2.48
5.269	BeO	40	16.07	0.45	4.96	1.55	−1.05	1.69		
		65	7.77	0.24	5.07	0.84	4.81	0.90		
		85	5.89	0.29	4.80	1.05	3.37	0.91		
5.240	BeO	40	22.84	0.54	8.54	1.85	2.35	1.95		
		65	12.58	0.29	6.47	1.03	4.94	1.08		
		85	9.96	0.34	8.64	1.22	5.75	1.07		
5.105	BeO	40	5.55	0.96	1.92	2.56				
		65	4.77	0.60	1.14	1.64				
		85	2.94	0.34	0.82	1.06				
2.793	BeO	40	2.06	0.18	−0.16	0.66	0.20	0.74		
		65	2.38	0.16	1.84	0.56	1.49	0.58		
		85	1.85	0.18	0.74	0.65	0.46	0.67		
2.741	BeO	40	10.58	0.32	−3.67	0.91				
		65	6.75	0.31	−0.42	0.87				
		85	5.29	0.34	1.44	1.02				
2.313	BeO	40	36.99	0.59						
		65	30.94	0.50						
		85	26.08	0.55						
2.154	CH_2	40	13.68	0.49	0.49	1.45				
(+)		65	10.87	0.59	8.62	1.53				
2.124		85	10.82	0.56	11.03	1.75				
2.000	CH_2	40	28.88	0.41						
		65	22.85	0.40						
		85	21.17	0.45						

cross section. The second, due to the transformation from laboratory to c.m. values of the gamma-ray angles, would be less than 2.5% for the worst case.

Seltzer[3] has estimated absolute detector efficiencies for gamma rays with energies from 2 to 20 MeV incident on the detector employed in the present measurements. His results for photopeak efficiencies have been used for the gamma-ray lines of interest in this work except for the 5.105- and 15.10-MeV lines. Seltzer's computations additionally provided an estimate of the absolute detector efficiency for 15.10-MeV gamma rays for the integral energy range from 14.08 to 15.10 MeV that was subsequently normalized to the energy range from 12.26 to 15.10 MeV, where the fits were performed. Analysis of the photopeaks and first-escape peaks of the strong, narrow lines at 6.129, 5.269, and 5.240 MeV, observed in the present work, indicated a systematic difference (about 10%) between the cross sections derived using Seltzer's first-escape and photopeak efficiencies. This 10% correction has been applied to the measured 5.105-MeV gamma-ray production cross sections.

The values of the detector efficiencies and the solid angle subtended by the detector include systematic uncertainties which could not be quantitatively estimated *a priori*. For this and other reasons, it was decided in advance to normalize a selected measured gamma-ray production cross section to a published value for the corresponding excitation cross section that is believed to be well determined. The total excitation cross section for the reaction $^{12}C(p,p')^{12}C^*(4.439)$ was estimated from the differential cross section of Stovall and Hintz[14] to be 42.9 ± 1.0 mb for 39.8-MeV protons and should be equal to the 4.438-MeV gamma-ray production cross section. The normalization factor that assures this equality is then 1.3 ± 0.2. This factor has been included in the normalized gamma-ray production cross sections presented in Table III.

For confirmation, the gamma-ray production cross section for the reaction $^{16}O(p,\gamma_{6.129})p'\,^{16}O$ was estimated from reported values of the excitation cross sections for the reactions $^{16}O(p,p')^{16}O^*(6.130$ and $8.872)$ for 39.7-MeV protons.[15] When these were combined with an estimate of the 11.080-MeV excitation cross section and the known branching ratios, the 6.129-MeV gamma-ray production cross section was estimated to be 34.8 ± 2.0 mb for 40-MeV protons. The normalization factor for this cross section is also 1.3 ± 0.2. Equality with the ^{12}C normalization factor indicates that the major sources of systematic errors have probably been eliminated. The same factor results in a normalized differential 15.10-MeV gamma-ray production cross section of 0.13 ± 0.03 mb/sr for the reaction $^{12}C(p,\gamma_{15.10})p'\,^{12}C$ for 40-MeV protons at 90 deg to the proton beam, in excellent agreement with the value of 0.12 ± 0.02 mb/sr reported by Measday *et al.*[16]

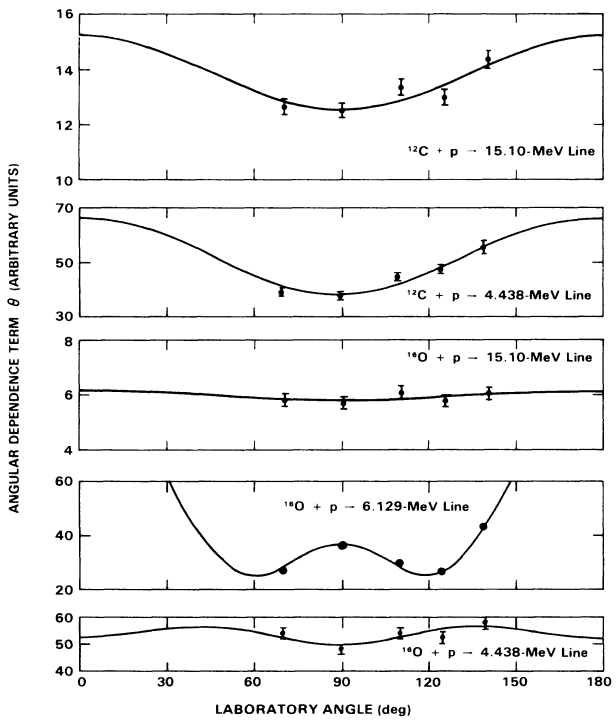

FIG. 7. Angular distributions of the angular-dependent portion of selected differential cross sections. All data and curves are for 40-MeV incident protons. The circles represent the present measurements of the angular-dependence term, in the same arbitrary units for all plots, for the five observation angles. The solid curves show the results of a least-squares fit of the data to a sum of Legendre polynomials. The coefficients for these fits and others not shown are presented in Table II.

V. RESULTS: GAMMA-RAY PRODUCTION CROSS SECTIONS

A. $^{12}C(p,\gamma_{15.10})p'\,^{12}C$

Normalized measurements of this cross section are presented in Table III and also in Fig. 8. The shaded region in Fig. 8 represents the confidence interval for the total gamma-ray production cross section estimated from reported 90 deg differential cross sections for 16.7- to 48.5-MeV protons[16] and for 14- to 20-MeV protons,[17] assuming isotropic emission. The open circles in Fig. 8 represent estimates of the 15.10-MeV gamma-ray production cross section made from reported measurements of the 15.11-MeV excitation cross section. The excitation cross sections have been reported for proton energies of 19.5,[17] 20.5—30.3,[18] 22.5—45,[19] 31.1,[20] 46,[21] 62,[22] and 185 MeV,[23] and have been corrected for the gamma-ray branching ratio of 0.9.

In 1979 the gamma-ray and excitation cross sections reported in the literature for this reaction were summarized.[2] In that work, the gamma-ray production cross sections[16,17] were normalized to the excitation cross section for 21-MeV protons[18] by multiplying by 0.9 and 0.8, respectively. This normalization is not necessary to reconcile the gamma-ray and excitation cross sections. The observed systematic differences, at least near 40 MeV, are almost certainly due to anisotropic gamma-ray emission.

TABLE III. Total gamma-ray production cross sections for protons incident on the indicated target and producing the indicated gamma-ray line. The first column gives the energy of the gamma-ray line and the second column gives the target material. The next three columns indicate the most probable excited nuclei, initial states, and final states involved in the transitions. The first set of cross sections, labeled "As measured," are the cross sections determined directly from the data. The second set, labeled "Normalized," have been normalized to published cross sections that are believed to be well determined. The numbers in parentheses are the uncertainties in the last two (or three) digits of the indicated cross section.

E_γ (MeV)	Target	Excited nucleus; spin and parity of initial and final states			Total gamma-ray production cross section (mb) As Measured 40 MeV	65 MeV	85 MeV	Normalized 40 MeV	65 MeV	85 MeV
15.10	BeO	^{12}C	1^+	0^+	0.368(39)	0.182(19)	0.159(18)	0.479(89)	0.237(44)	0.206(39)
15.10	CH_2	^{12}C	1^+	0^+	1.343(180)	0.790(106)	0.574(78)	1.75(36)	1.03(21)	0.75(15)
4.438	BeO	^{12}C	2^+	0^+	23.9(27)	a	a	31.1(59)	a	a
4.438	CH_2	^{12}C	2^+	0^+	34.3(48)	13.1(19)	8.8(13)	44.5(93)[b]	17.0(36)	11.5(25)
6.129	BeO	^{16}O	3^-	0^+	27.0(33)	10.5(13)	9.5(13)	35.1(69)	13.6(27)	12.3(25)
5.269	BeO	^{15}N	$\frac{5}{2}^+$	$\frac{1}{2}^-$	8.82(101)	4.27(49)	3.23(39)	11.47(220)	5.55(107)	4.20(82)
5.240	BeO	^{15}O	$\frac{5}{2}^+$	$\frac{1}{2}^-$	12.45(141)	6.86(77)	5.43(63)	16.2(31)	8.9(17)	7.1(14)
5.105	BeO	^{14}N	2^-	1^+	4.38(91)	3.79(65)	2.32(38)	5.70(148)	4.92(114)	3.02(68)
2.793	BeO	^{14}N	2^-	0^+	0.543(75)	0.628(78)	0.487(70)	0.71(15)	0.82(16)	0.63(13)
2.741	BeO	^{16}O	2^-	3^-	2.74(30)	1.75(20)	1.37(17)	3.56(67)	2.27(44)	1.78(35)
2.313	BeO	^{14}N	0^+	1^+	8.36(88)	6.99(74)	5.90(63)	10.9(20)	9.1(17)	7.7(14)
2.154 (+) 2.124	CH_2	^{10}B / ^{11}B	1^+ / $\frac{1}{2}^-$	3^+ / $\frac{3}{2}^-$	4.70(65)	3.74(54)	3.72(53)	6.11(127)	4.86(103)	4.83(102)
2.000	CH_2	^{11}C	$\frac{1}{2}^-$	$\frac{3}{2}^-$	9.50(128)	7.52(102)	6.96(95)	12.4(25)	9.8(20)	9.1(19)

[a]No cross sections since templates could be computed only for 40-MeV incident protons.
[b]This value is normalized to a well-determined cross section (see text).

B. $^{16}O(p,\gamma_{15.10})x^{12}C$

The normalized cross sections for this reaction are presented in Table III and are plotted in Fig. 8. Preliminary measurements of the ratio of this cross section to the cross section for the direct process, $^{12}C(p,\gamma_{15.10})p'\,^{12}C$, indicated that this ratio was comparable to the analogous ratio for producing 4.438-MeV gamma rays from the same targets.[24] This ratio at 40 MeV for 15.10-MeV gamma rays is 0.275 ± 0.058, while for 4.438-MeV gamma rays the ratio is significantly larger (0.697 ± 0.125). These ratios were taken to be equal for an investigation of the spectral parameters of energetic protons responsible for 4.438- and 15.10-MeV line fluences from solar flares.[2] The results presented here will alter the values of the spectral parameters originally determined in that work.

C. $^{16}O(p,\gamma_{6.129})p'\,^{16}O$

Normalized measurements of the cross sections for this reaction are presented in Table III and in Fig. 9. The crosses in Fig. 9 represent reported measurements of this cross section for proton energies of 8—23,[25] 25 and 44,[26] 12.1, 28.2, 48.3, and 145,[27] and 146 MeV.[28] The cross sections measured with NaI detectors[27,28] very likely include contributions due to unresolved gamma rays from the single-nucleon knockout reactions $^{16}O(p,\gamma_{6.322})pp^{15}N$ and $^{16}O(p,\gamma_{6.175})x^{15}O$.

The open circles in Fig. 9 represent estimates of the 6.129-MeV gamma-ray production cross section made from reported excitation cross sections for the 6.130-, 8.872-, and 11.080-MeV levels, correcting for the branching ratios.[29,30] Because the 3^+ state at 11.080 MeV cannot be resolved in (p,p') reactions from the 4^+ state at 11.095 MeV (which does not decay significantly through the 6.130-MeV level), only the sum of the two excitation cross sections has been reported in the literature. Suzuki,[31] based on his calculations, has reported that the principal component of the wave function of both states consists of alpha-particle motion with $l=2$ about the 2^+ excited state of ^{12}C. For this reason, it has been assumed in this work that the cross sections for excitation of these two states are equal. Measurements of the 6.130-MeV excitation cross section have been reported for proton energies of 17.0 and 18.8,[32] 19,[33] 23.4—46.1,[15] 135,[34,35] and 177 MeV.[36] Measurements of the 8.872-MeV excitation cross sections have been reported for proton energies of 17.0 and 18.8,[32] 19,[33] 23.4—46.1,[15] 42.5 and 44,[37] and 135 MeV.[34] Measurements of the sum of the 11.080- and 11.096-MeV excitation cross section have been reported for 19-MeV (Ref. 33) and 135-MeV (Ref. 34) protons.

D. $^{12}C(p,\gamma_{2.000})x^{11}C$, $^{12}C(p,\gamma_{2.154})x^{10}B + {}^{12}C(p,\gamma_{2.124})pp^{11}B$, and $^{12}C(p,\gamma_{4.438})p'\,{}^{12}C$

The first high-resolution measurements of the cross sections for the reaction $^{12}C(p,\gamma_{2.000})x^{11}C$ and for the sum of the cross sections for the reactions $^{12}C(p,\gamma_{2.154})x^{10}B$ and $^{12}C(p,\gamma_{2.124})pp^{11}B$ are presented in Table III. The latter two are not completely resolved, but the ^{10}B line is considerably weaker than the ^{11}B line. Previously reported measurements of cross sections for a line near 2 MeV were attributed entirely to the ^{11}C line,[27] but the NaI detector employed almost certainly could not resolve the three lines. While the sum of the present measurements of these cross sections are systematically lower than the previous measurements,[27] they are in agreement to within the experimental uncertainties.

Normalized cross sections for the reaction $^{12}C(p,\gamma_{4.438})p'\,{}^{12}C$ also are presented in Table III and are shown in Fig. 10. The crosses in Fig. 10 represent reported measurements of this cross section for proton energies of 6–23,[25] 14.6, 30.3, 50.3, and 145,[27] and 143 MeV.[38] The excitation cross sections for the 4.439-MeV level are equal to the 4.438-MeV gamma-ray production cross sections, and are represented as open circles in Fig. 10 for proton energies of 31.1,[20] 39.8,[14] 49.5,[39] 99.5,[40] 100,[41] 182,[36] and 185 MeV.[23] With two exceptions,[40,27] the results of all workers are remarkably consistent with a power-law decrease of the cross section with energy above 15 MeV.

It has been suggested[42] that the difference between the previously reported gamma-ray production cross sections[27] and the excitation cross sections above about 25 MeV was due to the unresolved contribution of gamma rays from the $^{12}C(p,\gamma_{4.444})pp^{11}B$ reaction. The measurements of the $^{11}C(\gamma_{2.000})$ and $^{11}B(\gamma_{2.124})+{}^{10}B(\gamma_{2.154})$ cross sections reported in the present work allow an estimate of the $^{11}B(\gamma_{4.444})$ cross section to be made.

Evidence[43] from a $^{12}C(p,2p)^{11}B^*$ experiment for 50-MeV incident protons suggests that the dominant mechanism at this energy is proton knock-out. In the absence of gamma-ray cascades from higher levels the $^{11}B(\gamma_{4.444})$ cross section is related to that for $^{11}B(\gamma_{2.124})$ by

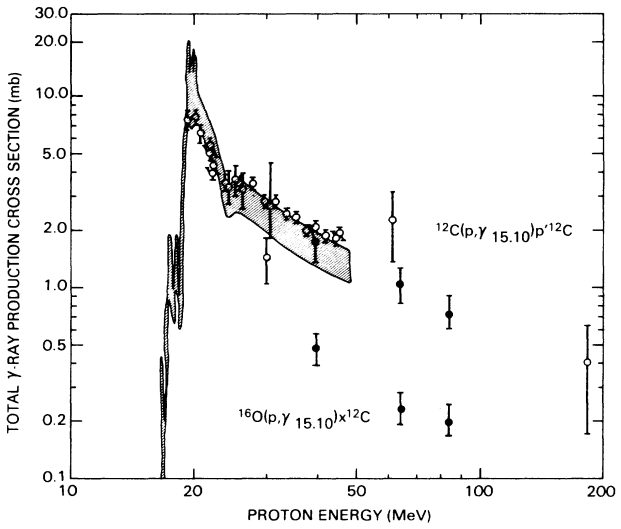

FIG. 8. Production cross sections for 15.10-MeV gamma rays as a function of incident proton energy for the reactions $^{12}C(p,\gamma_{15.10})p'\,{}^{12}C$ (upper points and shaded region) and $^{16}O(p,\gamma_{15.10})x^{12}C$ (the lower three solid circles *only*). The upper three solid circles represent the present measurements for the CH_2 target. The shaded region represents the ±20% confidence interval of the differential gamma-ray production cross section measured at 90 deg by Measday *et al.* (Ref. 16) and Warburton and Funsten (Ref. 17), multiplied by 4π sr for comparison with the total cross sections obtained in the present work. This neglects the fact that the gamma rays are not necessarily emitted isotropically. Angular fits to the present data for 40-, 65-, and 85-MeV incident protons indicate significant anisotropy in the gamma-ray emission. The apparent discrepancy between the excitation cross sections and the gamma-ray production cross sections could be explained by the degree of anisotropy observed. The open points represent measurements of the $^{12}C(p,p')^{12}C^*(15.11)$ excitation cross section, multiplied by the branching ratio for 15.10-MeV gamma rays of 0.9. References for the excitation cross sections are given in the text.

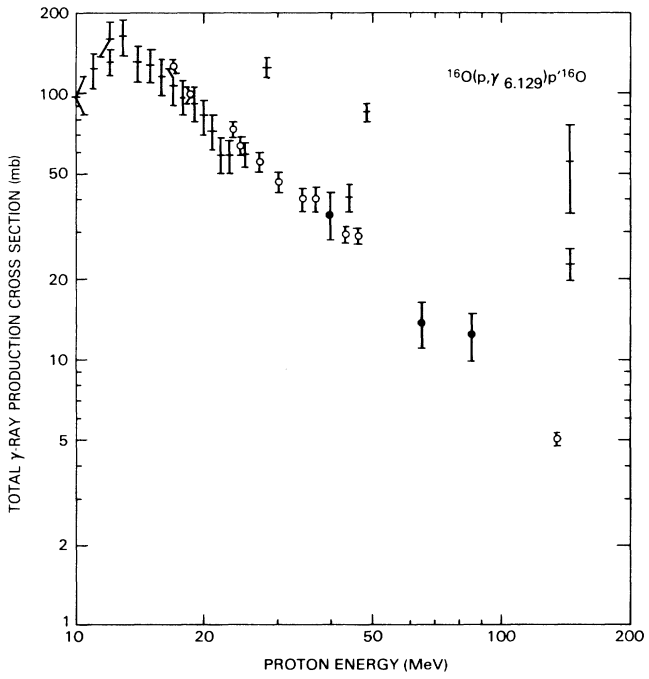

FIG. 9. Production cross sections for 6.129-MeV gamma rays as a function of incident proton energy for the reaction $^{16}O(p,\gamma_{6.129})p'\,{}^{16}O$. The present measurements of the gamma-ray production cross sections are represented by solid circles. The crosses represent previously reported measurements of the gamma-ray production cross section. The open circles represent an estimate of the gamma-ray production cross sections derived from the 6.130-, 8.872-, and 11.080-MeV excitation cross sections. See text for further explanation and references.

$$\sigma[^{12}\mathrm{C}(\mathrm{p},\gamma_{4.444})\mathrm{pp}^{11}\mathrm{B}] \cong \frac{C^2[\mathrm{p}+^{11}\mathrm{B}^*(4.445)]}{C^2[\mathrm{p}+^{11}\mathrm{B}^*(2.125)]} \times \sigma[^{12}\mathrm{C}(\mathrm{p},\gamma_{2.124})\mathrm{pp}^{11}\mathrm{B}] \ . \quad (7)$$

From Table III of Ref. 44 the value 0.3 is obtained for the ratio of the spectroscopic factors for 100-MeV incident protons. This value, when multiplied by the sum of the normalized cross sections for $^{11}\mathrm{B}(\gamma_{2.124})$ and $^{10}\mathrm{B}(\gamma_{2.154})$ from Table III of the present work, yields an estimate of the $^{11}\mathrm{B}(\gamma_{4.444})$ cross section of 1.8 mb for 40-MeV protons. Consideration of the effect of cascades from higher levels (see Table IV) feeding both the $^{11}\mathrm{B}^*(4.445)$ and $^{11}\mathrm{B}^*(2.125)$ levels lowers this estimate to 1.22 ± 0.25 mb. Even this value is an upper limit, because the contribution of $^{10}\mathrm{B}(\gamma_{2.154})$ has not been removed. A similar estimate is obtained after replacing the $^{11}\mathrm{B}(\gamma_{2.124})$ cross section by the product of σ_{pp}/σ_{pn} and the resolved $^{11}\mathrm{C}(\gamma_{2.000})$ cross section, where σ_{pp} and σ_{pn} are the total proton-proton and proton-neutron cross sections, respectively.

An estimate of the total cross section for the $^{12}\mathrm{C}(\mathrm{p},\gamma_{4.438})\mathrm{p}'^{12}\mathrm{C}$ reaction for 40-MeV protons based on previous measurements of the differential cross section at 135 deg (Ref. 27) and corrected for the anisotropy measured in the present work is 58.4 ± 4.6 mb. This is 15.6 ± 4.7 mb higher than the 42.9 ± 1.0 mb estimated from the reported excitation cross section.[14] This difference cannot be accounted for by the $^{12}\mathrm{C}(\mathrm{p},\gamma_{4.444})\mathrm{pp}^{11}\mathrm{B}$ reaction.

TABLE IV. Relative cross sections for exciting the lowest five states in $^{11}\mathrm{B}$ through the $^{12}\mathrm{C}(\mathrm{p},2\mathrm{p})^{11}\mathrm{B}^*$ reaction.

State J^π	Energy (MeV)	$\sigma(E_N)/\sigma(2.125)$
$\frac{1}{2}^-$	2.125[a]	1
$\frac{3}{2}^-$	4.445[a]	0.3
$\frac{5}{2}^-$	5.020[a]	1
$\frac{1}{2}^+$	6.792[b]	2.3
$\frac{7}{2}^-$	6.743[a]	0.18

[a]Table 3 of Ref. 44.
[b]Figure 8 of Ref. 43.

E. $^{16}\mathrm{O}(\mathrm{p},\gamma_{4.438})\mathrm{x}^{12}\mathrm{C}$

The normalized cross section for this spallation reaction was obtained only for 40-MeV protons and is presented in Table III and is also plotted in Fig. 11 along with previously reported cross sections for proton energies of

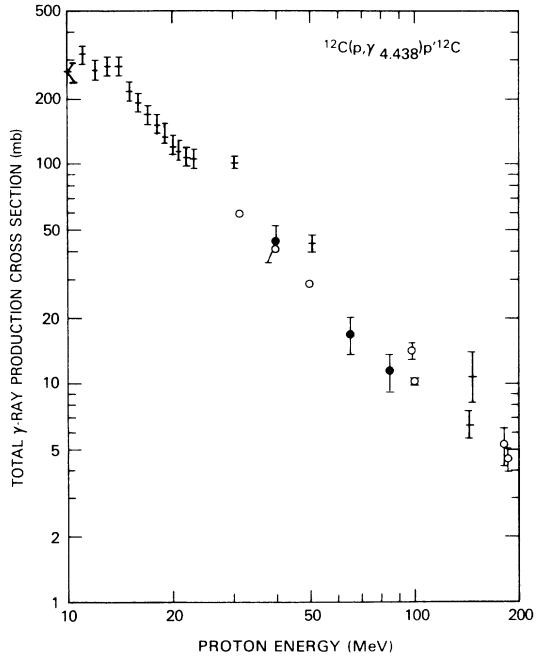

FIG. 10. Production cross section for 4.438-MeV gamma rays as a function of incident proton energy for the reaction $^{12}\mathrm{C}(\mathrm{p},\gamma_{4.438})\mathrm{p}'^{12}\mathrm{C}$. The present measurements are represented by solid circles. The crosses represent previously reported measurements of the gamma-ray production cross section. The open circles represent measurements of the scattered protons in the (p,p') reaction, integrated to give total excitation cross sections which, for the 4.439-MeV state of $^{12}\mathrm{C}$, are equal to the 4.438-MeV gamma-ray production cross section. References are given in the text.

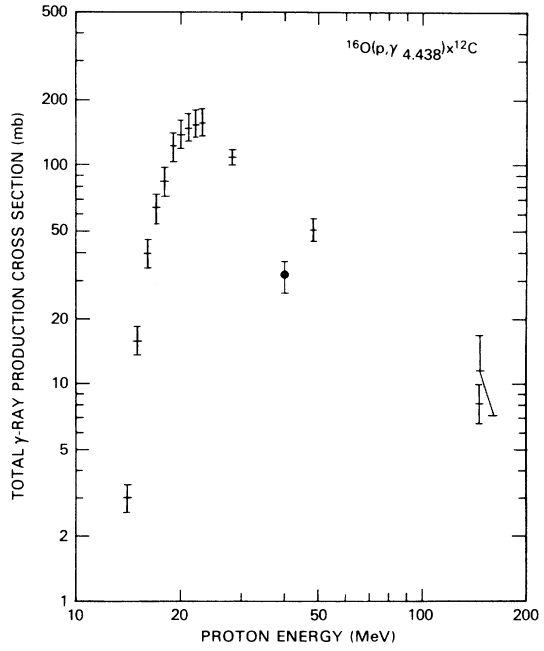

FIG. 11. Production cross section for 4.438-MeV gamma rays as a function of incident proton energy for the reaction $^{16}\mathrm{O}(\mathrm{p},\gamma_{4.438})\mathrm{x}^{12}\mathrm{C}$. The present measurement is represented by a solid circle. The crosses represent previously reported measurements of the gamma-ray production cross section. References are given in the text.

14—23,[25] 12.1, 28.2, 48.3, and 145,[27] and 146 MeV (the lower of the two points[28]). The cross section for 40-MeV protons estimated from the previously reported measurements[27] is 66.0±4.7 mb, significantly higher than the value measured in the present work.

An independent estimate of the cross section for 45-MeV protons can be obtained directly from the α_1 widths and the (p,p') cross sections as follows:

$$\sigma = \left[\sum_N \frac{\Gamma_{\alpha_1}(E_N)}{\Gamma_{\text{tot}}(E_N)} \sigma(40°, E_N) \right] \times \int d\Omega_c \frac{\sigma(\theta_c,\ 21\text{—}27\ \text{MeV})}{\sigma(40°,\ 21\text{—}27\ \text{MeV})} . \quad (8)$$

The integral is performed over all solid angles and the sum is over all ^{16}O excited states that contribute to the reaction (see Table I). The estimate of the cross section made this way is $26.6^{+8.7}_{-4.6}$ mb and is in good agreement with the normalized value for 40-MeV incident protons. The angular distribution of $\sigma(\theta_c)$ for $21 \leqq E_N \leqq 27$ MeV (Ref. 7) was used to carry out the integral. The confidence region was estimated by calculating the contribution to the cross section for states above 16 MeV with $\Gamma_{\alpha_1}/\Gamma_{\text{tot}} = 0.5$ and 0.25.

F. ^{16}O(p,$\gamma_{5.269}$)pp^{15}N, ^{16}O(p,$\gamma_{5.240}$)x^{15}O, and ^{16}O(p,$\gamma_{5.105}$)x^{14}N

The normalized cross sections for these three reactions, which produce intrinsically narrow gamma-ray lines, are presented in Table III. The two Doppler-broadened lines from ^{15}N and ^{15}O at 5.298 and 5.182 MeV, respectively, were not resolved. Measurements of the cross section for a line near 5.2 MeV have been reported.[27] In that work it was suggested that this line was an unresolved blend of the 5.269- and 5.298-MeV lines from states of ^{15}N and of the corresponding lines from mirror states in ^{15}O. It is likely that, in addition to these four lines, the 5.105-MeV line from the ^{16}O(p,$\gamma_{5.105}$)x^{14}N reaction contributed to the single reported line. The cross section for this unresolved line[27] is estimated to be 58.2±4.9, 34.8±4.9, and 24.4±5.3 mb, for 40-, 65-, and 85-MeV protons, respectively. If the three resolved cross sections reported in Table III are summed, the corresponding cross sections are 33.4±4.1, 19.4±2.3, and 14.3±1.8 mb. Some, if not all, of the difference between these sets of cross sections is due to the two unresolved lines.

A cross section of 2.6±0.7 mb for a gamma-ray line at 5.25 MeV has been reported for 146-MeV incident protons.[28] In that work it was also suggested that the gamma rays arose from the four lines of ^{15}O and ^{15}N near 5.25 MeV. If the sum of the three resolved cross sections obtained in the present work is extrapolated to 146 MeV, a value of 7.7±3.5 mb is obtained, which is statistically consistent with the previously reported measurement.

G. ^{16}O(p,$\gamma_{2.793}$)x^{14}N*(2.313), ^{16}O(p,$\gamma_{2.313}$)x^{14}N and ^{16}O(p,$\gamma_{2.741}$)p' ^{16}O*(6.130)

The normalized cross sections for these three reactions are presented in Table III. The 2.793-MeV gamma rays arise from the transition from the 5.106-MeV level of ^{14}N to the 2.313-MeV level. The branching ratio for this decay is 0.194±0.012, while the ratio for decay to the ground state is 0.799±0.010.[45] If the present 2.793- and 5.105-MeV cross sections are divided by the corresponding branching ratios, the resulting cross sections are statistically consistent.

The 2.313-MeV gamma rays can be produced from the direct reaction ^{16}O(p,$\gamma_{2.313}$)x^{14}N as well as through cascades from higher levels. The 3.948-MeV level decays 96.1% of the time to the 2.313-MeV level, producing a 1.635-MeV gamma ray. This peak is clearly observed in the measured pulse-height spectra, but cross sections cannot be measured because the line is not sufficiently resolved. Note that the 5.106-MeV state provides a contribution of about 10% to the 2.313-MeV cross section.

Previously reported measurements of cross sections for a line near 2.3 MeV were attributed to the ^{16}O(p,$\gamma_{2.365}$)x^{13}N reaction.[27] Cross sections for 40-, 65-, and 85-MeV protons can be estimated from those measurements to be 9.5±3.1, 6.4±1.8, and 5.1±1.5 mb, respectively. These values are in reasonable agreement with the present 2.313-MeV cross sections. For this reason, the suggestion[42] that the authors of Ref. 27 did not measure gamma rays from the decay of ^{13}N but from the decay of ^{14}N is probably correct.

The 2.741-MeV gamma rays arise from the transition from the 8.872-MeV level of ^{16}O to the 6.130-MeV level, with a branching ratio of 0.760±0.030.[8] Excitation cross sections for the reaction ^{16}O(p,p')^{16}O*(8.872) have been reported for protons with energies from 23 to 46 MeV.[15] For 40-MeV protons, this cross section is 3.2±0.3 mb (see Fig. 4 of Ref. 15). This value, multiplied by the branching ratio, gives an estimate of the contribution of the direct excitation of the 8.872-MeV level to the 2.741-MeV gamma-ray production cross section of 2.4±0.2 mb. As expected, this is somewhat lower than the present value.

VI. SUMMARY AND CONCLUSIONS

In this work, the gamma-ray production cross sections for a number of lines resulting from interactions of protons with ^{12}C and ^{16}O targets have been measured for incident proton energies of 40, 65, and 85 MeV. These cross sections are presented in Table III. The measured gamma-ray production cross sections from the present experiment for the most important lines, either by virtue of their high gamma-ray energy, such as the 15.10-MeV line, or by virtue of their large production cross sections, such as the 6.129-MeV and 4.438-MeV lines, are compared with earlier measurements in Figs. 8—11. An accurate knowledge of these cross sections from threshold to proton energies of 100 MeV or greater is important for the interpretation of a wide variety of space physics observations.

The present measurements of the cross section for the reaction $^{12}C(p,\gamma_{15.10})p'\,^{12}C$, shown in Fig. 8, are seen to be in excellent agreement with the values derived from the 15.11-MeV excitation cross sections. The cross sections for the reaction $^{16}O(p,\gamma_{15.10})x^{12}C$, also plotted in the same figure, are the first such measurements reported in the literature. At the given energies this cross section is approximately 25% that of the $^{12}C(p,\gamma_{15.10})p'\,^{12}C$.

The present $^{16}O(p,\gamma_{6.129})p'\,^{16}O$ cross sections, plotted in Fig. 9, follow closely the trend of previously reported measurements that were obtained with semiconductor detectors,[25,26] except perhaps the value for 44-MeV protons.[26] That value was corrected for contributions due to the second escape peak from the decay of the level at 7.117 MeV, but was not corrected for contributions due to the $^{16}O(p,\gamma_{6.175})x^{15}O$ reaction. These corrections were unnecessary in the present work because the 6.129-MeV line is much narrower than the other two. The cross section for the 6.175-MeV gamma-ray line can be estimated to be around 15 mb, almost exactly the difference between the previously reported[26] gamma-ray production cross section and the excitation cross section for 44-MeV protons. The set of reported measurements of the 6.129-MeV cross section for proton energies of 28.2, 48.3, and 145 MeV (Ref. 27) tend to be about a factor of 3 higher than other values and should not be compared directly with them as they were made with a NaI detector which could not resolve the $^{16}O^*(6.130)$ line from the strongly excited $^{15}N^*(6.324)$ line as well as the $^{15}O^*(6.176)$ line.

The present measurement of the cross section for the reaction $^{12}C(p,\gamma_{4.438})p'\,^{12}C$ for 40-MeV protons was normalized to the 43 ± 1 mb excitation cross section[14] at the same energy. In Sec. V D, it was shown that there are no significant contributions from unresolved lines, particularly the suggested[42] 4.444-MeV line from $^{11}B^*(4.445)$. Previous measurements of the cross section for the $^{12}C(p,\gamma_{4.438})p'\,^{12}C$ reaction for proton energies of 30.3, 50.3, and 145 MeV (Ref. 27) are about a factor of 1.5 higher than the corresponding excitation cross sections. This difference amounts to 22 ± 4 mb for 40-MeV protons and far exceeds the 1.2 mb estimated in this work for the $^{12}C(p,\gamma_{4.444})pp^{11}B$ reaction.

The previous measurement of the cross section for the reaction $^{16}O(p,\gamma_{4.438})x^{12}C$ for 48.3-MeV protons[27] is higher by about a factor of 2 than the present measurement at 40 MeV (see Fig. 11). Because this reaction produces three or more particles in the final state, excitation cross section measurements are incomplete. The effort required in making a complete kinematic determination is prohibitive. The raw data collected for the present experiment for 65- and 85-MeV protons await the calculation of a "template," which requires differential cross sections for inelastic proton scattering to $^{16}O^*$ at similar incident proton energies that are not currently available.

Murphy[46] has studied relative isotopic abundances at the site of solar flares using spectra measured with the Gamma-Ray Spectrometer (GRS) on board the Solar Maximum Mission (SMM) satellite. He concludes that the most likely site of the gamma-ray production is in the solar chromosphere and that the abundances of ^{12}C and ^{16}O at this site are lower than those in the solar photosphere by factors of 3 or 4. The latter result is insensitive to the assumed particle spectrum.[46] This suppression has also been observed by Meyer, who investigated previously reported extreme ultraviolet (EUV) and x-ray observations and suggested that the deficit may be caused by charge-dependent mass transport from the photosphere to the corona based on first-ionization potential.[47] For a typical proton spectrum,[46] the use of the present gamma-ray production cross sections implies an increase of about 25% in the ^{12}C and ^{16}O abundances when compared with abundances derived[46] using previous measurements.[27] This increase is not sufficient to account for the reported abundance deficits.

Future observations of high-energy gamma rays from solar flares will provide an opportunity to investigate the accelerated-particle spectrum and, with a knowledge of the intrinsic line shapes from this work and work in progress, the directionality of accelerated particles. This, in turn, can be used to gain information about the acceleration mechanism. A thorough knowledge of relevant cross sections and line shapes is critical for the interpretation of such spectra. The gamma-ray production cross sections for the reactions $^{12}C(p,\gamma_{4.438})p'\,^{12}C$ and $^{12}C(p,\gamma_{15.10})p'\,^{12}C$ are now reasonably well determined for proton energies up to 200 and 100 MeV, respectively. This is not the case for the production of the same lines from ^{16}O. The results obtained in the present work indicate that the flux ratio of 4.438- to 15.10-MeV gamma rays is significantly different for the two nuclei, so that the flux ratio produced in solar flares is both abundance and proton-spectrum dependent. Crannell, Crannell, and Ramaty parametrized the expected proton spectrum as a power law with spectral index s and a low-energy cutoff E_c. For a fixed value of the observed gamma-ray flux ratio and for typical values of the proton spectral parameters ($E_c=20$ MeV and $s=3$), changes in the $^{16}O(p,\gamma_{4.438})x\,^{12}C$ cross section of $\pm20\%$ (the uncertainty in the present measurement) would imply spectral indices of 2.7 ($+20\%$) and 3.3 (-20%). In order for the 4.438- and 15.10-MeV flux measurements to be a more sensitive diagnostic of the accelerated-particle spectrum in solar flares, both the 4.438- and 15.10-MeV gamma-ray production cross sections must be more precisely determined.

ACKNOWLEDGMENTS

The possibility of obtaining the measurements reported here using the University of Maryland Cyclotron was first recognized and brought to the attention of two of the authors (C.J.C. and J.I.T.) by Dr. N. S. Wall, Professor of Physics at the University of Maryland, who participated in and encouraged this work until his unexpected death. His key role at the inception of these efforts is gladly acknowledged, and his continued participation as a friend and collaborator is sadly missed. The efforts of the cyclotron administration and staff in providing accelerator time and data-acquisition facilities are gratefully acknowledged. The germanium detector employed in these measurements was provided by Princeton Gamma Tech (PGT) under time constraints which were extraordinarily severe. The cooperation and responsiveness of the PGT

staff are, likewise, sincerely appreciated. Additional assistance was provided by a number of individuals whose contributions are acknowledged as follows. Dr. N. R. Yoder was indispensible in providing help with software programming for data acquisition at the cyclotron. Mr. S. M. Seltzer calculated the response of the detector employed in this work to gamma rays with energies throughout the range of interest. Dr. L. G. Evans, assisted by Ms. J. V. Stoakes, applied HYPERMET for reduction of the raw spectral data. Further assistance with data acquisition and reduction was supplied by Dr. M. J. Bielefeld, Dr. J. R. Lapides, Dr. C. Samantha, Mr. R. L. Schmadebeck, Dr. L. W. Wo, Dr. L. I. Yin, Mr. D. Okamoto, Mr. C. Wade, and several enthusiastic summer students. Dr. H. Crannell and Dr. J. R. Calarco participated in valuable discussions on experimental technique and the physics of the nuclear transitions being studied. Two of us (F.L.L. and C.W.W.) gratefully acknowledge support for this work provided in part through NASA Grant NSG 5066.

[1]E. L. Chupp, in *Annual Review of Astronomy and Astrophysics*, edited by G. Burbidge, D. Layzer, and J. G. Phillips (Annual Reviews, Inc., Palo Alto, CA, 1984), p. 359.
[2]C. J. Crannell, H. Crannell, and R. Ramaty, Astrophys. J **229**, 762 (1979).
[3]S. M. Seltzer, private communication.
[4]F. L. Lang, C. W. Werntz, C. J. Crannell, J. I. Trombka, and C. C. Chang, NASA Technical Memorandum No. 87787, 1986.
[5]J. J. Kolata, R. Auble, and A. Galonsky, Phys. Rev. **162**, 957 (1967).
[6]M. B. Epstein, J. R. Quinn, S. N. Bunker, J. W. Verba, and J. R. Richardson, Nucl. Phys. **A169**, 337 (1971).
[7]M. Buenerd, P. Martin, P. de Saintignon, and J. M. Loiseaux, Phys. Rev. C **14**, 1316 (1976).
[8]F. Ajzenberg-Selove, Nucl. Phys. **A375**, 1 (1982).
[9]K. H. Bray, A. D. Frawley, T. R. Ophel, and F. C. Barker, Nucl. Phys. **A288**, 334 (1977).
[10]P. Martin and T. R. Ophel, Nucl. Phys. **A202**, 257 (1973).
[11]A. D. Frawley, K. H. Bray, and T. R. Ophel, Nucl. Phys. **A294**, 161 (1978).
[12]J. I. Trombka and R. L. Schmadebeck, Nucl. Instrum. Methods **62**, 253 (1968).
[13]G. W. Phillips and K. W. Marlow, Nucl. Instrum. Methods **137**, 525 (1976).
[14]T. Stovall and N. M. Hintz, Phys. Rev. **135**, B330 (1964).
[15]S. M. Austin, P. J. Locard, S. N. Bunker, J. M. Cameron, J. R. Richardson, J. W. Verba, and W. T. H. van Oers, Phys. Rev. C **3**, 1514 (1971).
[16]D. F. Measday, P. S. Fisher, A. Kalmykov, F. A. Nikolaev, and A. B. Clegg, Nucl. Phys. **45**, 98 (1963).
[17]E. K. Warburton and H. O. Funsten, Phys. Rev. **128**, 1810 (1962).
[18]D. K. Scott, P. S. Fisher, and N. S. Chant, Nucl. Phys. **A99**, 177 (1967).
[19]H. V. Geramb, K. Amos, R. Sprickmann, K. T. Knöpfle, M. Rogge, D. Ingham, and C. Mayer-Böricke, Phys. Rev. C **12**, 1697 (1975).
[20]J. K. Dickens, D. A. Haner, and C. N. Waddell, Phys. Rev. **129**, 743 (1963).
[21]E. L. Petersen, I. Slaus, J. W. Verba, R. F. Carlson, and J. R. Richardson, Nucl. Phys. **A102**, 145 (1967).
[22]K. A. Amos, H. V. Geramb, R. Sprickmann, J. Arvieux, M. Buenerd, and G. Perrin, Phys. Lett. **52B**, 138 (1974).
[23]D. Hasselgren, P. U. Renberg, O. Sundberg, and G. Tibell, Nucl. Phys. **69**, 81 (1965).
[24]J. R. Lapides, C. J. Crannell, H. Crannell, W. F. Hornyak, S. M. Seltzer, J. I. Trombka, and N. S. Wall, NASA Technical Memorandum No. 79560, 1978.
[25]P. Dyer, D. Bodansky, A. G. Seamster, E. B. Norman, and D. R. Maxson, Phys. Rev. C **23**, 1865 (1981).
[26]J. Narayanaswamy, P. Dyer, S. R. Faber, and S. M. Austin, Phys. Rev. C **24**, 2727 (1981).
[27]W. Zobel, F. C. Maienschein, J. H. Todd, and G. T. Chapman, Nucl. Sci. Eng. **32**, 392 (1968).
[28]K. J. Foley, G. L. Salmon, and A. B. Clegg, Nucl. Phys. **31**, 43 (1962).
[29]R. E. Pixley and W. Benenson, Nucl. Phys. **A91**, 177 (1967).
[30]M. C. Bertin and R. E. Pixley, Nucl. Phys. **A150**, 247 (1970).
[31]Y. Suzuki, Prog. Theor. Phys. **55**, 1751 (1976).
[32]W. W. Daehnick, Phys. Rev. **135**, B1168 (1964).
[33]W. F. Hornyak and R. Sherr, Phys. Rev. **100**, 1409 (1955).
[34]K. Amos, W. Bauhoff, I. Morrison, S. F. Collins, R. S. Henderson, B. M. Spicer, G. G. Shute, V. C. Officer, D. W. Devins, D. L. Friesel, and W. P. Jones, Nucl. Phys. **A413**, 255 (1984).
[35]J. Kelly, W. Bertozzi, T. N. Buti, F. W. Hersman, C. Hyde, M. V. Hynes, B. Norum, F. N. Rad, A. D. Bacher, G. T. Emery, C. C. Foster, W. P. Jones, D. W. Miller, B. L. Berman, W. G. Love, and F. Petrovich, Phys. Rev. Lett. **45**, 2012 (1980).
[36]H. Tyrén and T. A. J. Maris, Nucl. Phys. **4**, 637 (1957).
[37]G. Perrin, D. Lebrun, J. Chauvin, P. Martin, P. De Santignon, D. Eppel, H. V. Geramb, H. L. Yadav, and V. A. Madsen, Phys. Lett. **68B**, 55 (1977).
[38]A. B. Clegg, K. J. Foley, G. L. Salmon, and R. E. Segel, Proc. Phys. Soc. (London) **78**, 681 (1961).
[39]J. A. Fannon, E. J. Burge, D. A. Smith, and N. K. Ganguly, Nucl. Phys. **A97**, 263 (1967).
[40]K. Strauch and F. Titus, Phys. Rev. **103**, 200 (1956).
[41]Y. S. Horowitz and R. E. Bell, Can. J. Phys. **48**, 201 (1970).
[42]R. Ramaty, B. Kozlovsky, and R. E. Lingenfelter, Astrophys. J. Suppl. Ser. **40**, 487 (1979).
[43]H. G. Pugh, D. L. Hendrie, M. Chabre, E. Boschitz, and I. E. McCarthy, Phys. Rev. **155**, 1054 (1967).
[44]D. W. Devins, D. L. Friesel, W. P. Jones, A. C. Attard, I. D. Svalbe, V. C. Officer, R. S. Henderson, B. M. Spicer, and G. G. Shute, Aust. J. Phys. **32**, 323 (1979).
[45]F. Ajzenberg-Selove, Nucl. Phys. **A449**, 1 (1986).
[46]Ronald Murphy, Ph.D. thesis, University of Maryland, 1985.
[47]J. Meyer, Astrophys. J. Suppl. Ser. **57**, 173 (1985).